Faraday
Discussions

Accepted Manuscript

Faraday Discussions

Royal Society of Chemistry

ROYAL SOCIETY OF CHEMISTRY

www.rsc.org/faraday_d

1

2

3

The characterisation of diesel exhaust particles – composition, size distribution and partitioning

7

Mohammed S. Alam[1], Soheil Zeraati-Rezaei[2], Christopher P. Stark[1], Zhirong Liang[2], Hongming Xu[2] and Roy M. Harrison[1]*†

[1] Division of Environmental Health and Risk Management
School of Geography, Earth and Environmental Sciences
University of Birmingham
Edgbaston, Birmingham B15 2TT
United Kingdom

[2] School of Mechanical Engineering
University of Birmingham
Edgbaston, Birmingham B15 2TT
United Kingdom

22

23

* To whom correspondence should be addressed.
Tele: +44 121 414 3494; Fax: +44 121 414 3708; Email: r.m.harrison@bham.ac.uk

† Also at: Department of Environmental Sciences / Center of Excellence in Environmental Studies, King Abdulaziz University, PO Box 80203, Jeddah, 21589, Saudi Arabia

Abstract

A number of major research questions remain concerning the sources and properties of road traffic generated particulate matter. A full understanding of the composition of primary vehicle exhaust aerosol and its contribution to secondary organic aerosol (SOA) formation still remains elusive, and many uncertainties exist relating to the semi-volatile component of the particles. Semi-Volatile Organic Compounds (SVOC) are compounds which partition directly between the gas and aerosol phases under ambient conditions. The SVOC in engine exhaust are typically hydrocarbons in the C_{15}-C_{35} range, and are largely uncharacterised because they are unresolved by traditional gas chromatography and form a large hump in the chromatogram referred to as Unresolved Complex Mixture (UCM).

In this study, thermal desorption coupled to comprehensive two dimensional Gas-Chromatography Time-of-Flight Mass-Spectrometry (TD-GC×GC-ToF-MS) was exploited to characterise and quantify the composition of SVOC from the exhaust emission. Samples were collected from the exhaust of a diesel engine, sampling before and after a diesel oxidation catalyst (DOC), while testing at steady state conditions. Engine exhaust was diluted with air and collected using both filter and impaction (nano-MOUDI), to resolve total mass and size resolved mass respectively. Adsorption tubes were utilised to collect SVOC in the gas phase and analysed using thermal desorption, while particle size distribution was evaluated by sampling with a DMS500.

The SVOC was observed to contain predominantly *n*-alkanes, branched alkanes, alkyl-cycloalkanes, alkyl-benzenes, PAH and various cyclic aromatics. Particle phase compounds identified were similar to those observed in engine lubricants, while vapour phase constituents were similar to those measured in fuels. Preliminary results are presented illustrating differences in the particle size distribution and SVOC composition when collecting samples with and without a DOC. The results indicate that the DOC tested is of very limited efficiency, under the studied engine operating conditions, for removal of SVOC, especially at the upper end of the molecular weight range.

54   **1.0   Introduction**

55   Urban air pollution is comprised of a highly complex mixture of compounds both in the vapour and

56   particulate phase. These complex mixtures can enter the atmosphere through various natural and

57   anthropogenic processes such as incomplete combustion of fossil fuels, biomass burning and forest

58   fires and may also be formed as products of gas to particle conversion through atmospheric

59   reactions. Urban areas therefore, provide a natural focus for research on air quality as they

60   experience high emissions from space heating and road transport associated with their high

61   population densities.[1] Road traffic generated particulate matter (PM) has gained major interest over

62   the last few decades owing to their associated detrimental impacts on human health.[2-4] PM

63   emissions from road vehicles can be generated from exhaust and non-exhaust emission types; for

64   example, exhaust tailpipe and abrasion of vehicle parts including brakes, clutch and tyres, and re-

65   suspension of dust.[5] There are currently more than 37 million vehicles on UK roads. In 1994 the UK

66   diesel passenger cars comprised 7.4% of the fleet and increased to 34.5% of the total by 2013.[6] This

67   means that approximately 1 in 3 light duty vehicles in the UK use diesel engines. Furthermore, in

68   2014, 50% of all new registration vehicles in the UK were diesel, while 48% were petrol and 2% were

69   alternative fuel vehicles. This increase in diesel engines has led to predictions that diesel fuel will be

70   the number one transport fuel in the world by 2020.[7]

71   Primary vehicle exhaust emissions can exist in the gas phase or as liquids or solids in aerosols, where

72   the partitioning between the phases is determined by the compound's vapour pressure, its

73   occurrence as a pure substance or as a mixture in the condensed phase and its water solubility. Once

74   emitted into the atmosphere the compounds with vapour pressures of $>10^{-5}$ atm, $10^{-5} - 10^{-11}$ atm

75   and $<10^{-11}$ atm, at ambient temperature are expected to be volatile (in the gas phase), semi volatile

76   and non-volatile (in the condensed phase), respectively. A semi-volatile organic compound (SVOC)

77   includes any compound with >1% of its mass in both the condensed and vapour phases.[8] The

78   composition of primary vehicle exhaust aerosol and its contribution to secondary organic aerosol

79   (SOA) formation still remains elusive, where many uncertainties exist relating to the semi-volatile

80   component of the particles.

81   Diesel exhaust particles consist mainly of agglomerated solid carbonaceous material and ash,

82   together with organic and sulphur containing compounds.[9] The solid carbon is formed during

83   combustion and is subsequently oxidised, while a small fraction of the fuel and motor/lubricating oil

84   are not oxidised and are emitted as VOC/SVOCs in the exhaust. The fraction associated with

85   unburned fuel and lubricating oil is known to vary with engine design and operating conditions,

86   ranging from <10 % to >90 %.[9] Many studies have investigated the composition of the organic

87   fraction of the particles, reporting targeted groups of compounds such as aliphatic-alkanes, cyclic-

88   alkanes, polycyclic aromatic hydrocarbons (PAH), steranes and hopanes.[10-14] Limited studies,

89   however, focus on higher carbon number species ($>C_{15}$) owing to instrumental/experimental

90   limitations.[15, 16] The SVOC in diesel exhaust emissions are typically hydrocarbons in the $C_{15} - C_{25}$

91   range, and are largely uncharacterised because they are unresolved by traditional gas

92   chromatography and form a large hump in the chromatogram referred to as Unresolved Complex

93   Mixture (UCM). To add further complexity, the composition of exhaust aerosol is also dependent

94   upon the sampling collection method. When collecting diesel exhaust aerosol, it is diluted and

95   cooled, which leads to the transformation of gas phase volatile species in the tail pipe into solid and

96   liquid PM.[17, 18] Dilution and cooling processes therefore determine the relative amounts of species

97   that adsorb and/or condense onto existing particles and nucleate to form new particles.[19-21]

98   The size distribution of diesel PM has been extensively studied.[9, 21-27] The majority of the particle

99   mass exists in the $100 - 300$ nm diameter range (accumulation mode) and is where the

100   carbonaceous agglomerates and associated adsorbed materials are found. Approximately $1 - 20\%$ of

101   the particle mass and $>90\%$ of the particle number exists in the $5 - 50$ nm diameter range

102   (nucleation mode) and is where the volatile organic and sulphur containing compounds that form

103   during exhaust dilution and cooling are assumed to reside.[9] Particles with diameter >2.5 µm (coarse

104   mode) comprise typically 20-50% of the particle mass in the PM_{10} size range. The physico-chemical

105   properties of particles influence their residence time in the atmosphere, and determine their surface

106   area which governs their availability for atmospheric reactions, optical properties of particles will

107   influence atmospheric visibility and light scattering, and human health effects.

108   This paper presents the use of thermal desorption coupled to comprehensive two dimensional Gas-

109   Chromatography Time-of-Flight Mass-Spectrometry (TD-GC×GC-ToF-MS) to characterise and

110   quantify the composition of SVOC from diesel exhaust emissions, both in the gas and particulate

111   phases. The composition was also investigated for different particle size fractions using collection by

112   cascade impaction (nano-MOUDI), while particle number size distribution was evaluated by sampling

113   with a DMS500.

114   **2.0   Experimental**

115   ***2.1 Engine sampling***

116   Experiments were conducted with a light-duty diesel engine; 2.2 L, 4-cylinder in-line compression

117   ignition (CI) engine equipped with a common rail direct injection system, a variable-nozzle-turbine

118   (VNT) turbocharger and a diesel oxidation catalyst (DOC). The open engine control unit (Open-ECU)

119   allows full control over the engine operating parameters. A schematic of the engine testing system is

120   illustrated in Figure 1.

121   30 min samples were collected at steady state engine operating conditions at a load of 5.9 bar brake

122   mean effective pressure (BMEP) and speed of 1800 revolutions per minute (RPM), before and after

123   the DOC. Fuel injection pressure was maintained at 1000 bar and a pilot-main fuel injection strategy

124   was used. Exhaust gas recirculation (EGR) percentage was fixed at 12%. Sampling was started after

125   ensuring that the engine was fully warmed-up and thermally stable. Standard European, EN590

126   specifications, ultra-low sulphur diesel (ULSD, S<10ppm) and 5W-30 part synthetic engine lubricating

127   oil were used for the experiments. Particulate number and size distribution were measured by a

128   Cambustion DMS500 MKII fast particulate analyser and averaged over 1 minute for each sample – 4

129   samples per experiment. A schematic of the in-house exhaust dilution and sample collection system

130   is shown in Figure 2.

131   The dilution system incorporates a modified TSI 3302A diluter. The diluter was modified to use

132   cleaned compressed air by using a high flow rate moisture trap and two HEPA filters. The undiluted

133   hot exhaust sample was delivered via a heated line maintained at 191°C and subsequently mixes

134   with the dilution air at ambient temperature. The dilution ratio (DR) was kept at 1:30±5 confirmed

135   by measurements of nitric oxide (NO) before and after the dilution system. The diluted sample was

136   divided into two flow streams, (see Figure 2, labelled 1 and 2). A flow rate of 9 L/min was fixed for

137   stream 1, created by a vacuum pump. A calibrated rotameter and needle valve combination was

138   used to measure the flow rate, and was removed while sampling to avoid particle losses. The second

139   rotameter downstream of the adsorption tube was fixed to ensure the flow rates remained constant

140   throughout the engine sampling period. A nano-Micro Orifice Uniform Deposit Impactor

141   (nanoMOUDI) 125 instrument (MSP Copley Scientific, UK) was utilised for collecting different size

142   particles via this flow stream. The nanoMOUDI has fourteen stages with nominal 50% cut-points of

143   10,000, 5600, 3200, 1800, 1000, 560, 320, 180, 100, 56, 32, 18, 10 and <10 nm. The sample was

144   collected for 30 min, using polypropylene backed PTFE 47 mm filters (Whatman, Maidstone, UK).

145   Stream 2, demonstrated a fixed flow rate of 1.8 L/min. Stainless steel thermal adsorption tubes

146   packed with 1cm quartz wool, 300mg Carbograph 2TD 40/60 (Markes International) were used to

147   collect gas phase constituents from stream 2; downstream of a polypropylene backed PTFE 47 mm

148   filter (Whatman, Maidstone, UK) to remove any particulates. The temperatures at the sampling

149   points were 25±5°C.

150

151   *2.3 Analytical instrumentation*

152   Adsorption tubes were desorbed using thermal desorption (Unity 2, Markes International,

153   Llantrisant, UK) and samples were subsequently analysed using a gas chromatograph (GC, 7890A,

154   Agilent Technologies, Wilmington, DE, USA) equipped with a Zoex ZX2 cryogenic modulator

155   (Houston, TX, USA). The first dimension was equipped with a SGE DBX5, non-polar capillary column

156   (30 m, 0.25 mm ID, 0.25 μm – 5% phenyl polysilphenylene-siloxane), and the second dimension

157   column equipped with a SGE DBX50 (4.0 m, 0.1 mm ID, 0.1 μm – 50% phenyl polysilphenylene-

158   siloxane). The GC×GC was interfaced with a Bench-ToF-Select, time-of-flight mass spectrometer

159   (ToF-MS, Markes International, Llantrisant, UK). The scan speed was 50 Hz with a mass range of 35

160   to 600 *m/z*. Ionisation energies that were explored in this work were 14 eV and 70 eV. All data

161   produced were processed using GC Image v2.3 (Zoex Corporation, Houston, US).

162

163   *2.2 Analysis of samples*

164   The filters were spiked with 50 μL of 1ng/ μL deuterated internal standards for quantification. Filters

165   were immersed in dichloromethane (DCM), ultrasonicated for 20 min at 20°C. The extract was

166   concentrated to 50 μL under a gentle flow of nitrogen for analysis using GC×GC-ToF-MS. 1 μL of the

167   extracted sample was injected in a split ratio 100:1 at 300°C. The initial temperature of the primary

168   oven (120°C) was held for 2 min and then increased at 2°C/min to 210°C, followed by 1.5°C/min to

169   325°C. The initial temperature of the secondary oven (120°C) was held for 2 min, and then increased

170   at 3°C/min to 200°C, followed by 2°C/min to 300°C and a final increase of 1°C/min to 330°C to

171   ensure all species passed through the column. The transfer line temperature was 330°C and the ion

172   source temperature was 280°C. Helium was used as the carrier gas at a constant flow rate of 1

173   mL/min.

174   Adsorption tubes were desorbed using TD. Briefly, the tubes were spiked with 1ng of deuterated

175   internal standard for quantification, and desorbed onto the cold trap at 350°C for 15 min (trap held

176   at 20°C). The trap was then purged onto the column in a split ratio of 102:1 at 350°C and held for 4

177   min. The initial temperature of the primary oven (90°C) was held for 2 min and then increased to

178   2°C/min to 240°C, followed by 3°C/min to 310°C and held for 5 min. The initial temperature of the

179   secondary oven (40°C) was held for 2 min and then increased at 3°C/min to 250°C, followed by an

180   increase of 1.5°C/min to 315°C and held for 5 min. Helium was used as the carrier gas at a constant

181   flow rate of 1 mL/min.

182

183   **3.0   Results and Discussion**

184   A typical two dimensional separation for diesel fuel and an engine lubricant is shown in Figure 3A

185   and B, respectively. All compounds were separated by volatility in the x-axis (first dimension) and by

186   polarity in the y-axis (second dimension). Peak identification was based on retention indices and

187   mass spectral data from the (National Institute of Standards and Technology) NIST library. The

188   GC×GC conditions for the two contour plots illustrated in Figure 3A and B are outlined in section 2.2,

189   similar to the filters, and are not optimum conditions for separating diesel or motor oil samples. The

190   purpose for this was to get an indication of the positioning of compounds in the contour plots that

191   are present in the filters and adsorption tubes that may come from diesel fuel and/or engine oil. A

192   detailed investigation of the separation of engine oils and diesel fuel using GC×GC-ToF-MS is given

193   elsewhere[28],[29, 30] Figure 3A shows that diesel fuel contains up to C_{20} compounds which are

194   represented in the first portion of the contour plot, whereas engine oil samples are dominated by

195    $C_{18} - C_{36}$ compounds forming a UCM in the latter portion of the contour plot (Figure 3B). The

196   presence of both these UCMs are observed in transient diesel engine exhaust filter samples using

197   the same GC×GC operating conditions (data not shown here) indicating the importance in identifying

198   constituents in diesel and lubricating oils, which are both precursors of engine exhaust emissions.

199   Sutton et al. (2005) isolated individual hydrocarbon fractions from a UCM of biodegraded crude oil

200   and suggested that the entire oil UCM could contain approximately 250,000 unidentified

201   compounds.[31]

202   Stainless steel thermal adsorption tubes were used to collect gas phase emissions and analysed

203   using TD-GC×GC-ToF-MS. The chromatogram for a 30 min sample collected at steady state engine

204   operating conditions at a load of 5.9 bar BMEP and speed of 1800 RPM, before the DOC is shown in

205   Figure 4. The 3D chromatographic image indicates an abundance of gas phase constituents up to $C_{22,}$

206   although *n*-alkanes are present up to C_{33} (RT_1 > 60 min, not shown in Figure 4). The chromatogram is

207   very similar to Figure 1A, the diesel fuel, indicating that the majority of the gas phase hydrocarbon

208   engine emission is from the diesel fuel. Recently, Dunmore et al. (2015) showed how diesel related

209   hydrocarbons could dominate gas phase reactive carbon in urban environments.[32] Their study

210   showed that approximately 60 % of the winter primary hydrocarbon hydroxyl radical reactivity was

211   from diesel related hydrocarbons and that they could contribute to up to 50 % of the ozone

212   production potential. The authors measured up to C_{13} and estimated the unmeasured diesel

213   emissions (up to C_{22}) using fuel composition-based emission factors from Gentner et al. (2013).[33]

214   Approximately 12,000 peaks were found in the chromatography illustrated in Figure 4(A) for the gas

215   phase samples compared to 8000 for the diesel fuel (Figure 1A). Compounds that were identified

216   include straight and branched alkanes ($C_{11} - C_{33}$) (Figure 4B), cycloalkanes ($C_{11} - C_{25}$) (Figure 4C), C9-

217   C12 aromatics (Figure 4D and 4E), naphthalenes (Figure 4F), as well as aldehydes, ketones, alkanoic

218   acids, alkyl benzenes, nitriles, alkyl phenyl ketones, alkyl-biphenyls, furans, furanones, decalins, PAH

219   and sulphur containing compounds including benzothiazole and diphenyl sulfone. Compounds not

220   found in the NIST library were further investigated and tentatively identified using the molecular

221   mass of species found at the same retention times from 14eV ionisation mass spectral data.

222   In addition to the qualitative data above, preliminary quantitative data for n-alkanes, n-

223   alkylcylohexanes and PAHs were calculated in order to be used as surrogates for modelling

224   evaporation and composition changes of traffic induced ultrafine particles.[34] These quantitative data

225   are shown in Table 1 for total PM (gas phase, particulate and total concentrations) and compared to

226   those data measured after the DOC. The DOC is designed to limit the amount of harmful emissions

227   released to the environment from diesel engines. Its primary functions are the oxidation of CO,

228   unburned hydrocarbons and NO, and can also provide some oxidation of soluble organic fraction

229   (SOF) components to improve soot filter performance.[35] Diesel oxidation catalysts typically reduce

230   emissions of PM by 20 – 40 % or more and gaseous emissions by 50 – 70 %.[36] Table 1 shows the

231   concentration reduction of n-alkanes when measuring these species after the DOC, with a total

232   percentage decrease for C_{11} to C_{33} of 19, 28 and 24 % in the vapour, particulate and the sum of the

233   vapour and particulate phases, respectively. These data, for alkanes, suggest that the efficiency of

234   the DOC for higher molecular weight compounds (HMW, *e.g.* >C_{28}), is less than for lower molecular

235   weight compounds (LMW). The total reduction of the sum of vapour and particulate phases for the

236   HMW ($C_{28} - C_{32}$) was <10 %. The results are, however, indicative of some re-partitioning of the

237   particulate component into the vapour phase.

238   The efficiency of reducing the particulate emissions for both n-alkylcyclohexanes and n-alkanes is

239   greater than for the gaseous phase. The n-alkylcyclohexane compounds show a total reduction of

240   19, 27 and 21 % after the DOC, for the vapour, particulate and the sum of the vapour and particulate

241   phases, respectively. For $C_{12} - C_{26}$ compounds the total (sum of vapour and particulate phase)

242   concentration reductions were 2592 to 2050 ng/m³. The concentration reductions of individual

243   compounds in the vapour phase are few, whereas all concentrations in the particulate phase are

244   reduced efficiently by >20 % (for LMW compounds, >C_{20}) and to a lesser extent for HMW (>5 % for

245   >C_{21}). Since the DOC is expected predominantly to adsorb and oxidise vapour, the results appear to

246   reflect very active re-partitioning between the particulate and vapour phases.

247   PAH concentrations illustrate a larger total reduction of 28, 26 and 27 % after the DOC for the

248   vapour, particulate and the sum of the vapour and particulate phases, respectively. This reduction is

249   more pronounced for the species that are more likely to be in the gas phase (NAP to ANT).[37, 38] The

250   greater reduction of ANT (68%) in comparison to other PAH in the presence of the DOC may explain

251   why roadside concentrations of ANT are generally low in the UK in comparison to some developing

252   countries.[39, 40] For HMW PAH (PYR to B(a)P) the efficiency of the DOC is reduced for the vapour

253   phase but appears efficient for the particulate phase (see Table 1).

254   A nanoMOUDI 125 instrument (MSP Copley Scientific, UK) was utilised for collecting different size

255   particles. Each of the fourteen stages of the nanoMOUDI with nominal 50% cut-points of 10,000,

256   5600, 3200, 1800, 1000, 560, 320, 180, 100, 56, 32, 18, 10 and <10 nm, were analysed using GC×GC-

257   ToF-MS. Approximately 1500 peaks were found in the majority of each of the 13 stage two-

258   dimensional chromatograms, using the blob detection technique performed by GC Image v2.3 (Zoex

259   Corporation, Houston, US) software, with a UCM similar to that found in Figure 1B, engine lubricant;

260   consistent with other studies.[41] Compounds identified included straight and branched chain alkanes

261   (C_{12} – C_{33}), cycloalkanes (C_{11} – C_{25}), alkyl benzenes, PAH, decalins, steranes and hopanes. Sulphur

262   containing compounds that were present in the gas phase were not observed in the particulate

263   phase. The concentration distribution of *n*-alkane compounds throughout the nanoMOUDI is shown

264   in Table 2. Interestingly, the largest concentrations were observed in different size fractions

265   according to MW. For example, for LMW compounds (C_{12} – C_{16}) the largest concentrations measured

266   were in the size fraction 1.0 μm in diameter, whereas for HMW compounds (C_{26} – C_{31}) the largest

267   concentrations were observed in the 0.1 μm diameter particle fraction.

268   The bold numbers in shaded grey are the largest concentrations found for those carbon number

269   species. There is a clear trend for the maximum concentration of the alkanes to be associated with

270   smaller particles as molecular weight increases. This is probably a consequence of the Kelvin effect

271   which increases the equilibrium vapour pressure, and hence volatility of compounds, as particle

272   surface curvature increases with diminishing particle size. Hence the more volatile lower molecular

273   weight compounds are destabilised, with an increased tendency to partition into the vapour phase

274   as particle size decreases. This result is consistent with the theoretical predictions made within the

275   FASTER project and with the results of thermodenuder experiments.[34, 42] Studies have suggested that

276   particles in the 5 – 100 nm diameter range consist mainly of HMW hydrocarbons associated with

277   engine lubricant,[10, 11] which is in broad agreement with the results in this study as the largest

278   concentrations for C_{32} and C_{33} are found in the smaller size ranges (56 nm diameter) compared to

279   other LMW alkanes (see Table 2).   Furthermore, roadside aerosol studies using hygroscopic, organic

280   and volatility Tandem Differential Mobility Analyser techniques have shown that particles in the

281   nucleation mode have partly evaporated leaving a 10 nm non-volatile core. [41]

282   The sum of the total size fractions indicates that the largest concentrations found in the PM are

283   found in the $C_{23} - C_{29}$ region, which also corresponds to the motor oil UCM region shown in Figure

284   1B. Schauer et al. (1999) reported that the gas phase portion of the UCM consisted of HMW SVOC,

285   which accounted for slightly less than half that of the total carbonyl mass emission rate, while the

286   particle phase portion of the UCM was similar to motor oil when analysed by GC/MS, consistent with

287   the results found in this study.[41] Figure 5 illustrates the gas/particle phase distribution of *n*-alkane

288   concentrations. A bimodal distribution is observed giving rise to a diesel ($<C_{20}$) source and an engine

289   lubricant ($C_{21} - C_{27}$) source. Elevated concentrations for the LMW alkanes exist in the gas phase,

290   while HMW ($>C_{24}$) are predominantly in the particle phase.

291

292   **4.0   Conclusion**

293   Thermal desorption coupled to comprehensive two dimensional Gas-Chromatography Time-of-Flight

294   Mass-Spectrometry (TD-GC×GC-ToF-MS) was exploited to characterise and quantify the composition

295   of SVOC from the exhaust emission. Samples were collected from the exhaust of a diesel engine,

296   before and after a diesel oxidation catalyst (DOC). This preliminary dataset shows that the SVOC was

297   observed to contain predominantly straight and branched alkanes ($C_{11} - C_{33}$), cycloalkanes ($C_{11} - C_{25}$),

298   various cyclic aromatics, PAH, decalins and alkyl benzenes. Sulphur containing compounds were

299   observed only in the gas phase, as were ketones, aldehydes and naphthalenes. Particle phase

300   compounds identified were similar to those observed in engine lubricants, while vapour phase

301   constituents were similar to those measured in fuels. Sampling after the DOC showed total

302   reductions of 19, 19 and 28 % for gas phase *n*-alkanes, alkyl-cyclohexanes and PAH, respectively;

303   although the DOC illustrated less efficiency for HMW compounds (in the gas phase). With current

304   DOC technology claiming 50 – 70 % reduction in emissions in the gas phase alone, this study shows

305   that there is large variation between compound classes and compounds within a compound class,

306   most probably due to reactivity.

307   Although studies have reported the size distribution and composition of fine PM emitted from diesel

308   engines, with chemical speciation such as sulphate, ammonium, nitrate, EC and OC;[43-45] or have

309   investigated gas and particle phase tailpipe emissions reporting VOC, SVOC and particle associated

310   OC,[41] very limited studies have investigated the organic composition of diesel exhaust emissions

311   corresponding to different size fractions.   We present the *n*-alkane ($C_{12} - C_{33}$) concentrations

312   measured in 13 different size fractions, showing an increase in the non-volatile concentration with

313   decreasing size fractions. The mode peak for different alkanes was found to be dependent upon

314   MW, with HMW concentrations peaking at 56 – 100 nm and LMW concentrations peaking at 1 µm.

315   Gas and particle phase distributions of alkanes were also presented showing an overall (total)

316   bimodal distribution, with > 70 % in the gas phase for compounds $\leq C_{20}$ and < 30 % for compounds $\geq$

317   C_{20}. The DOC tested is of very limited efficiency (4 – 68 % for the compounds measured); under the

318   studied engine operating conditions, and appears to cause substantial re-partitioning of compounds

319   from the condensed phase into vapour.

320

321   **5.0   Acknowledgements**

324

325   **6.0   References**

326   1.   R. M. Harrison, M. Dall'Osto, D. C. S. Beddows, A. J. Thorpe, W. J. Bloss, J. D. Allan, H. Coe, J.

327   R. Dorsey, M. Gallagher, C. Martin, J. Whitehead, P. I. Williams, R. L. Jones, J. M. Langridge,

328   A. K. Benton, S. M. Ball, B. Langford, C. N. Hewitt, B. Davison, D. Martin, K. F. Petersson, S. J.

329   Henshaw, I. R. White, D. E. Shallcross, J. F. Barlow, T. Dunbar, F. Davies, E. Nemitz, G. J.

330   Phillips, C. Helfter, C. F. Di Marco and S. Smith, *Atmospheric Chemistry and Physics*, 2012, **12**,

331   3065-3114.

332   2.   J. L. Mauderly, *Environmental Health Perspectives*, 1994, **102**, 165-171.

333   3.   M. Masiol, A. Hofer, S. Squizzato, R. Piazza, G. Rampazzo and B. Pavoni, *Atmospheric*

334   *Environment*, 2012, **60**, 375-382.

335   4.   J. Rissler, E. Swietlicki, A. Bengtsson, C. Boman, J. Pagels, T. Sandström, A. Blomberg and J.

336   Löndahl, *Journal of Aerosol Science*, 2012, **48**, 18-33.

337   5.   P. Pant and R. M. Harrison, *Atmospheric Environment*, 2013, **77**, 78-97.

338   6.   SMMT, *The Society of Motor Manufacturers and Traders - Motor Industry Facts 2015*, 2015.

339   7.   ExxonMobil, *The Outlook for Energy: A view to 2040, Tech. rep., Exxon Mobil Corporation,*

340   *Texas*, 2014.

341   8.   N. M. Donahue, A. L. Robinson, C. O. Stanier and S. N. Pandis, *Environmental Science &*

342   *Technology*, 2006, **40**, 2635-2643.

343   9.   D. B. Kittelson, *Journal of Aerosol Science*, 1998, **29**, 575-588.

344   10.   H. Sakurai, H. J. Tobias, K. Park, D. Zarling, K. S. Docherty, D. B. Kittelson, P. H. McMurry and

345   P. J. Ziemann, *Atmospheric Environment*, 2003, **37**, 1199-1210.

346   11.   H. J. Tobias, D. E. Beving, P. J. Ziemann, H. Sakurai, M. Zuk, P. H. McMurry, D. Zarling, R.
347   Waytulonis and D. B. Kittelson, *Environmental Science and Technology*, 2001, **35**, 2233-2243.
348   12.   J. J. Schauer, M. J. Kleeman, G. R. Cass and B. R. T. Simoneit, *Environmental Science and
349   Technology*, 1999, **33**, 1578-1587.
350   13.   B. Zielinska, J. Sagebiel, J. D. McDonald, K. Whitney and D. R. Lawson, *Journal of the Air &
351   Waste Management Association*, 2004, **54**, 1138-1150.
352   14.   L. Huang, S. V. Bohac, S. M. Chernyak and S. A. Batterman, *Atmospheric Environment*, 2015,
353   **102**, 228-238.
354   15.   A. W. H. Chan, G. Isaacman, K. R. Wilson, D. R. Worton, C. R. Ruehl, T. Nah, D. R. Gentner, T.
355   R. Dallmann, T. W. Kirchstetter, R. A. Harley, J. B. Gilman, W. C. Kuster, J. A. de Gouw, J. H.
356   Offenberg, T. E. Kleindienst, Y. H. Lin, C. L. Rubitschun, J. D. Surratt, P. L. Hayes, J. L. Jimenez
357   and A. H. Goldstein, *Journal of Geophysical Research: Atmospheres*, 2013, **118**, 6783-6796.
358   16.   G. Isaacman, K. R. Wilson, A. W. H. Chan, D. R. Worton, J. R. Kimmel, T. Nah, T. Hohaus, M.
359   Gonin, J. H. Kroll, D. R. Worsnop and A. H. Goldstein, *Analytical Chemistry*, 2012, **84**, 2335-
360   2342.
361   17.   B. Giechaskiel, M. Maricq, L. Ntziachristos, C. Dardiotis, X. Wang, H. Axmann, A. Bergmann
362   and W. Schindler, *Journal of Aerosol Science*, 2014, **67**, 48-86.
363   18.   M. Matti Maricq, *Journal of Aerosol Science*, 2007, **38**, 1079-1118.
364   19.   E. M. Lipsky and A. L. Robinson, *Environmental Science and Technology*, 2006, **40**, 155-162.
365   20.   A. L. Robinson, N. M. Donahue, M. K. Shrivastava, E. A. Weitkamp, A. M. Sage, A. P. Grieshop,
366   T. E. Lane, J. R. Pierce and S. N. Pandis, *Science*, 2007, **315**, 1259-1262.
367   21.   I. Abdul-Khalek, D. Kittelson and F. Brear, *SAE Technical Paper*, 1999, **1999-01-1142**.
368   22.   M. J. Kleeman, J. J. Schauer and G. R. Cass, *Environmental Science and Technology*, 2000, **34**,
369   1132-1142.
370   23.   A. Charron and R. M. Harrison, *Atmospheric Environment*, 2003, **37**, 4109-4119.
371   24.   J. Schneider, N. Hock, S. Weimer and S. Borrmann, *Environmental Science and Technology*,
372   2005, **39**, 6153-6161.
373   25.   A. Domínguez-Sáez, M. Viana, C. C. Barrios, J. R. Rubio, F. Amato, M. Pujadas and X. Querol,
374   *Environmental Science & Technology*, 2012, **46**, 11187-11194.
375   26.   T. Rönkkö, A. Virtanen, K. Vaaraslahti, J. Keskinen, L. Pirjola and M. Lappi, *Atmospheric
376   Environment*, 2006, **40**, 2893-2901.
377   27.   L. Pirjola, M. Karl, T. Rönkkö and F. Arnold, *Atmos. Chem. Phys.*, 2015, **15**, 10435-10452.
378   28.   M. S. Alam, C. Stark and R. M. Harrison, *Analytical chemistry*, 2015, **Submitted**.

379	29.	G. S. Frysinger and R. B. Gaines, *Journal of High Resolution Chromatography*, 1999, **22**, 251-
380		255.
381	30.	D. R. Gentner, G. Isaacman, D. R. Worton, A. W. H. Chan, T. R. Dallmann, L. Davis, S. Liu, D. A.
382		Day, L. M. Russell, K. R. Wilson, R. Weber, A. Guha, R. A. Harley and A. H. Goldstein,
383		*Proceedings of the National Academy of Sciences*, 2012, **109**, 18318-18323.
384	31.	P. A. Sutton, C. A. Lewis and S. J. Rowland, *Organic Geochemistry*, 2005, **36**, 963-970.
385	32.	R. E. Dunmore, J. R. Hopkins, R. T. Lidster, J. D. Lee, M. J. Evans, A. R. Rickard, A. C. Lewis and
386		J. F. Hamilton, *Atmos. Chem. Phys.*, 2015, **15**, 9983-9996.
387	33.	D. R. Gentner, D. R. Worton, G. Isaacman, L. C. Davis, T. R. Dallmann, E. C. Wood, S. C.
388		Herndon, A. H. Goldstein and R. A. Harley, *Environ Sci Technol*, 2013, **47**, 11837-11848.
389	34.	I. Nikolova, A. R. MacKenzie, X. Cai, M. S. Alam and R. M. Harrison, *Faraday Discussions*,
390		2015, **Submitted**.
391	35.	A. Russell and W. S. Epling, *Catalysis Reviews*, 2011, **53**, 337-423.
392	36.	T. V. Johnson, *SAE Technical Paper*, 2001, DOI: 10.4271/2001-01-0184.
393	37.	M. S. Alam, J. M. Delgado-Saborit, C. Stark and R. M. Harrison, *Atmospheric Chemistry and
394		Physics*, 2014, **14**, 2467-2477.
395	38.	I. J. Keyte, R. M. Harrison and G. Lammel, *Chem Soc Rev*, 2013, **42**, 9333-9391.
396	39.	M. S. Alam, J. M. Delgado-Saborit, C. Stark and R. M. Harrison, *Atmospheric Environment*,
397		2013, **77**, 24-35.
398	40.	M. A. Alghamdi, M. S. Alam, J. Yin, C. Stark, E. Jang, R. M. Harrison, M. Shamy, M. I. Khoder
399		and I. I. Shabbaj, *Science of The Total Environment*, 2015, **506–507**, 401-408.
400	41.	J. J. Schauer, M. J. Kleeman, G. R. Cass and B. R. T. Simoneit, *Environmental science &
401		technology*, 1999, **33**, 1578-1587.
402	42.	P. Tiitta, P. Miettinen, P. Vaattovaara, J. Joutsensaari, T. Petäjä, A. Virtanen, T. Raatikainen,
403		P. Aalto, H. Portin, S. Romakkaniemi, H. Kokkola, K. E. J. Lehtinen, M. Kulmala and A.
404		Laaksonen, *Atmospheric Environment*, 2010, **44**, 976-986.
405	43.	M. J. Kleeman, J. J. Schauer and G. R. Cass, *Environmental science & technology*, 2000, **34**,
406		1132-1142.
407	44.	M. A. Robert, M. J. Kleeman and C. A. Jakober, *Journal of the Air & Waste Management
408		Association*, 2007, **57**, 1429-1438.
409	45.	M. A. Robert, S. VanBergen, M. J. Kleeman and C. A. Jakober, *Journal of the Air & Waste
410		Management Association*, 2007, **57**, 1414-1428.

411

412   **Tables and Figures**

413   **Table 1.**   Concentrations of n-alkanes, n-alkylcyclohexanes and PAH in the vapour phase,
414   particulate phase and sum of vapour and particulate phase, before and after the
415   DOC, and their percentage reductions

416   **Table 2.**   Concentrations (ng/m3) of n-alkanes (C12 – C33) in the particulate phase size
417   fractions 10 μm to 0.01 μm measured using nano-MOUDI 125ii. The bold numbers in
418   shaded grey are the largest concentrations found for those carbon number species.

419   **Figure 1.**   Schematic of the engine testing system

420   **Figure 2.**   Schematic of the exhaust dilution and sample collection system.

421   **Figure 3.**   A two dimensional separation (contour plot) of **(A)** diesel fuel, and **(B)** engine
422   lubricant. X-axis separation on a volatility basis; y-axis separation on a polarity basis.
423   Each coloured spot represents an individual species and has a corresponding full
424   mass spectrum. The intense red spots are major peaks, while the blue spots
425   represent less abundant peaks.

426   **Figure 4.**   3 dimensional separations of gas phase constituents collected with an adsorption
427   tube and analysed using TD-GC×GC-ToF-MS. **(A)** Total ion chromatogram **(B)-(F)**
428   Selected ion chromatograms. The white solid line signifies 1D chromatography

429   **Figure 5.**   Gas/particle phase distribution of *n*-alkane concentration

Faraday Discussions Accepted Manuscript

n-Alkanes ($\mu g/m^3$)								
	Vapour phase		**% reduction**	**Particulate phase**		**% reduction**	**Total (v+p)**		**% reduction**
	Before DOC	After DOC		Before DOC	After DOC		Before DOC	After DOC	
C12	1.07	0.87	18%	0.15	0.05	70%	1.21	0.92	24%
C13	1.07	0.88	18%	0.47	0.30	37%	1.54	1.18	24%
C14	0.90	0.72	20%	0.44	0.28	37%	1.34	1.00	25%
C15	1.00	0.99	1%	0.50	0.27	46%	1.50	1.26	16%
C16	0.62	0.67	-8%	0.51	0.38	24%	1.13	1.05	7%
C17	0.34	0.46	-34%	0.32	0.14	57%	0.67	0.60	11%
C18	0.24	0.20	17%	0.36	0.26	27%	0.59	0.46	23%
C19	0.21	0.16	24%	0.22	0.16	27%	0.44	0.33	25%
C20	0.20	0.10	48%	0.26	0.20	21%	0.46	0.31	33%
C21	0.23	0.05	79%	0.31	0.25	21%	0.54	0.29	45%
C22	0.29	0.06	78%	0.26	0.22	16%	0.55	0.28	49%
C23	0.34	0.07	80%	0.31	0.18	41%	0.65	0.25	62%
C24	0.29	0.09	69%	0.26	0.24	9%	0.56	0.33	40%
C25	0.21	0.08	62%	0.48	0.37	22%	0.68	0.45	34%
C26	0.19	0.10	49%	0.45	0.32	29%	0.64	0.42	35%
C27	0.10	0.11	-8%	0.51	0.28	45%	0.61	0.39	36%
C28	0.10	0.15	-46%	0.49	0.39	21%	0.59	0.54	9%
C29	0.13	0.16	-26%	0.50	0.44	12%	0.63	0.60	4%
C30	0.08	0.14	-72%	0.49	0.41	17%	0.57	0.55	4%
C31	0.10	0.13	-38%	0.42	0.35	17%	0.52	0.48	7%
C32	0.07	0.08	-18%	0.33	0.30	8%	0.39	0.38	4%
C33	0.00	0.00	n/a	0.24	0.19	21%	0.24	0.19	21%
Total	*7.77*	*6.28*	*19%*	*8.28*	*5.97*	*28%*	*16.1*	*12.2*	*24%*
n-Alkyl-cyclohexanes (ng/m^3)								
C12	659.0	540.0	18%	0.0	0.0	n/a	659.0	540.0	18%
C13	295.0	161.0	45%	0.0	0.0	n/a	295.0	161.0	45%
C14	331.0	263.0	21%	33.4	15.1	55%	364.0	279.0	23%
C15	179.0	177.0	1%	61.2	35.6	42%	240.0	212.0	12%
C16	146.0	169.0	-16%	86.7	25.9	70%	233.0	195.0	16%
C17	57.0	49.0	14%	55.0	41.8	24%	112.0	91.0	19%
C18	29.0	35.0	-21%	27.1	12.4	54%	56.0	47.0	16%
C19	12.0	25.0	-108%	63.2	36.0	43%	75.0	61.0	19%
C20	11.0	15.0	-36%	52.1	41.8	20%	63.0	57.0	10%
C21	33.0	17.0	48%	67.7	64.1	5%	101.0	81.0	20%
C22	12.0	13.0	-8%	74.2	69.8	6%	87.0	83.0	5%
C23	37.0	24.0	35%	85.0	82.1	3%	122.0	106.0	13%
C24	14.0	18.0	-29%	58.6	50.0	15%	72.0	68.0	6%
C25	42.0	5.0	88%	49.0	46.1	6%	91.0	51.0	44%
C26	0.0	0.0	n/a	21.3	18.8	12%	21.0	19.0	10%
Total	*1857*	*1511*	*19%*	*734*	*539*	*27%*	*2592*	*2050*	*21%*
PAH (ng/m^3)								
NAP	402.0	281.0	30%	0.0	0.0	n/a	402.0	281.0	30%
ACEY	71.0	47.5	33%	0.0	0.0	n/a	71.0	47.5	33%
ACE	42.7	32.5	24%	0.0	0.0	n/a	42.7	32.5	24%
FLU	38.8	30.6	21%	0.0	0.0	n/a	38.8	30.6	21%
PHE	31.9	19.4	39%	1.5	1.2	23%	33.5	20.6	38%
ANT	38.3	12.2	68%	0.3	0.3	23%	38.6	12.4	68%
PYR	16.1	19.6	-21%	17.9	10.8	40%	34.0	30.4	11%
FLR	18.3	21.5	-17%	18.9	10.8	43%	37.1	32.3	13%
CHR	15.1	15.4	-2%	18.7	13.7	26%	33.7	29.1	14%
B(a)A	11.9	12.0	-1%	13.6	11.1	19%	25.5	23.1	10%
B(a)P	16.6	16.6	0%	8.9	7.5	16%	25.5	24.1	5%
B(ghi)P	0.0	0.0	n/a	30.2	26.5	12%	30.2	26.5	12%
Total	*702*	*508*	*28%*	*110*	*81.8*	*26%*	*812*	*590*	*27%*

430

Table 1. Concentrations of n-alkanes, n-alkylcyclohexanes and PAH in the vapour phase, particulate phase and sum of the vapour and particulate phase, before and after the DOC, and their percentage reductions

C number	Size Fractions (μm)														
	<0.010	0.010	0.018	0.032	0.056	0.10	0.18	0.32	0.56	1.0	1.8	3.2	5.6	10	TOTAL
	Concentrations (ng/m^3)														
C12	6.61	6.35	9.04	9.07	12.8	13.4	16.4	18.2	19.6	**20.3**	15.9	16.6	17.0	19.6	201.0
C13	4.15	5.19	7.44	8.28	9.72	7.88	15.7	14.4	19.7	**19.8**	16.5	15.7	16.8	19.6	181.0
C14	5.30	5.41	5.29	7.65	9.46	10.5	12.8	12.6	13.3	**19.4**	15.4	14.0	14.3	18.3	164.0
C15	5.06	5.20	6.55	6.46	6.70	8.13	10.7	12.4	14.8	**21.0**	13.7	11.7	13.9	14.8	151.0
C16	3.66	3.02	3.98	6.42	6.47	7.86	7.84	9.70	10.5	**13.5**	10.4	11.8	12.9	13.3	121.0
C17	4.28	4.54	2.71	4.56	5.74	5.92	8.54	11.0	**14.2**	7.83	10.2	10.6	10.9	12.7	114.0
C18	1.17	1.66	1.27	1.74	2.16	3.07	4.68	5.76	**10.7**	8.23	5.28	3.95	8.23	8.43	66.0
C19	1.89	2.69	2.10	2.69	3.52	3.30	5.64	5.97	**9.90**	8.31	5.30	4.52	5.24	5.21	66.0
C20	2.77	2.20	3.87	4.28	7.74	9.37	12.4	**16.0**	7.54	6.82	4.81	4.24	5.93	5.32	93.0
C21	3.22	2.42	4.96	6.11	9.56	12.0	**20.4**	15.1	9.04	5.60	6.64	6.22	6.18	7.29	115.0
C22	3.47	3.47	8.44	12.4	16.2	18.2	**24.2**	21.3	16.0	16.0	9.98	8.20	4.67	2.40	165.0
C23	8.07	6.33	9.53	15.8	17.9	26.1	**30.2**	26.5	17.7	22.4	18.3	9.16	8.60	2.62	219.0
C24	8.22	6.84	20.1	24.7	30.4	46.8	**53.4**	42.7	37.5	37.7	21.4	18.4	15.1	9.11	372.0
C25	11.1	13.1	28.7	33.4	32.6	45.8	**64.2**	47.1	28.4	42.0	30.9	26.0	9.60	11.2	424.0
C26	12.0	8.96	31.1	24.1	43.6	**53.3**	50.2	41.5	19.8	28.7	22.4	21.8	13.1	10.4	381.0
C27	7.78	8.16	28.9	33.3	46.9	**60.3**	55.8	38.8	17.6	30.0	9.54	17.6	8.44	7.78	371.0
C28	12.0	13.6	26.7	25.3	42.3	**51.6**	46.7	29.2	17.8	19.7	4.67	15.1	5.09	8.44	318.0
C29	16.8	26.8	31.1	44.4	36.2	**47.4**	28.0	22.3	12.0	3.99	3.98	19.1	3.30	2.68	298.0
C30	4.67	2.69	7.13	18.2	21.3	**30.1**	22.4	18.4	17.6	15.8	13.5	11.4	5.18	6.11	195.0
C31	2.77	5.17	6.83	10.2	16.7	**18.9**	16.5	17.5	6.83	6.68	8.35	7.00	3.42	1.70	129.0
C32	7.47	2.60	5.13	12.4	**18.5**	10.3	13.4	13.1	5.13	10.8	8.30	4.97	3.57	4.80	120.0
C33	7.06	8.38	7.79	13.8	**16.8**	11.1	9.47	9.10	7.93	7.62	5.91	4.65	2.94	6.18	119.0
Total	140.0	145.0	259.0	325.0	413.0	501.0	**530.0**	449.0	334.0	372.0	261.0	263.0	194.0	198.0	**4384.0**

Table 2. Concentrations (ng/m^3) of n-alkanes (C12 – C33) in the particulate phase size fractions 10 μm to 0.01 μm measured using nano-MOUDI 125ii. The bold numbers in shaded grey are the largest concentrations found for those carbon number species.
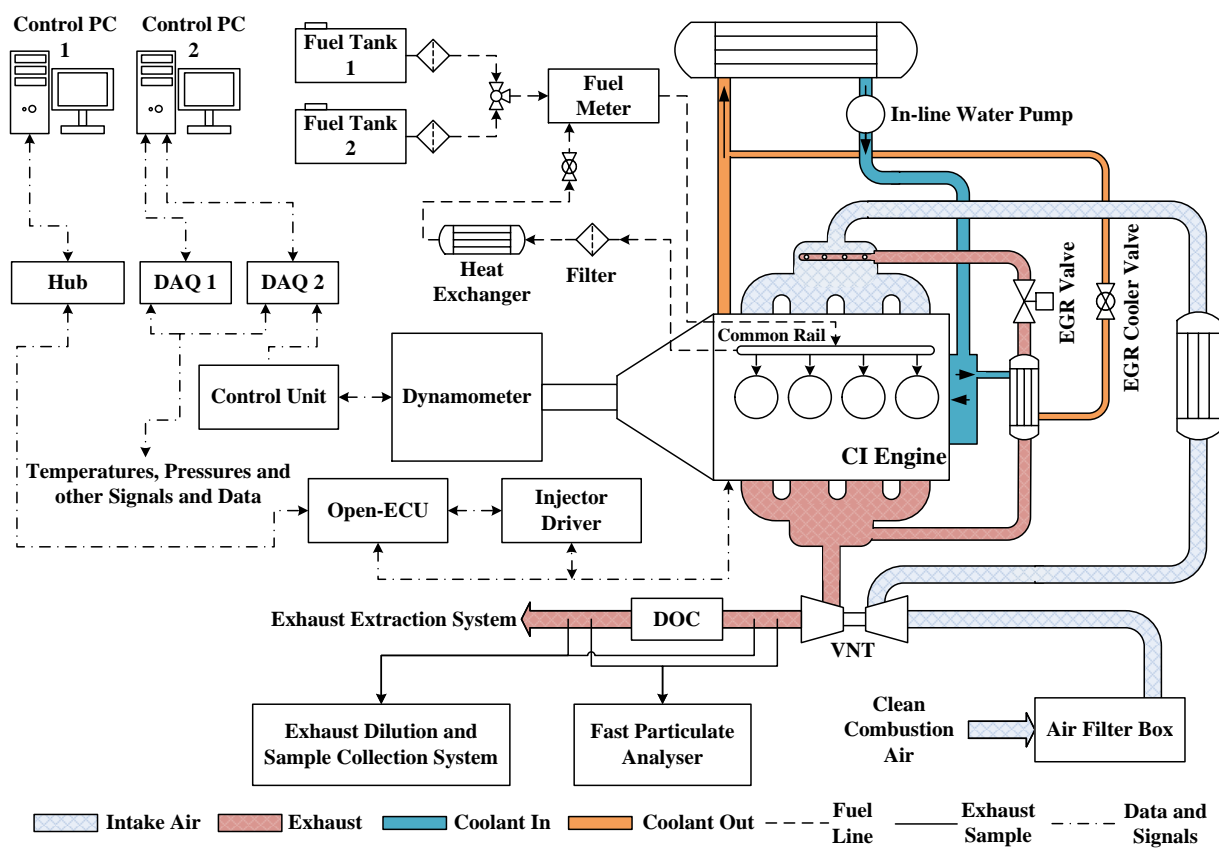
Control PC 1 Control PC 2

Fuel Tank 1 Fuel Tank 2

Fuel Meter

In-line Water Pump

Hub DAQ 1 DAQ 2

Heat Exchanger Filter

Common Rail

EGR Valve EGR Cooler Valve

Control Unit Dynamometer

CI Engine

Temperatures, Pressures and other Signals and Data

Open-ECU Injector Driver

Exhaust Extraction System DOC

VNT

Exhaust Dilution and Sample Collection System

Fast Particulate Analyser

Clean Combustion Air Air Filter Box

Intake Air   Exhaust   Coolant In   Coolant Out   Fuel Line   Exhaust Sample   Data and Signals

Figure 1. Schematic of the engine testing system

431

432

433

434

435

436

437

438

439

440

441

442

Figure 2. Schematic of the exhaust dilution and sample collection system.

443

444

445

446

447

448

449

450

451

452

453

454

455
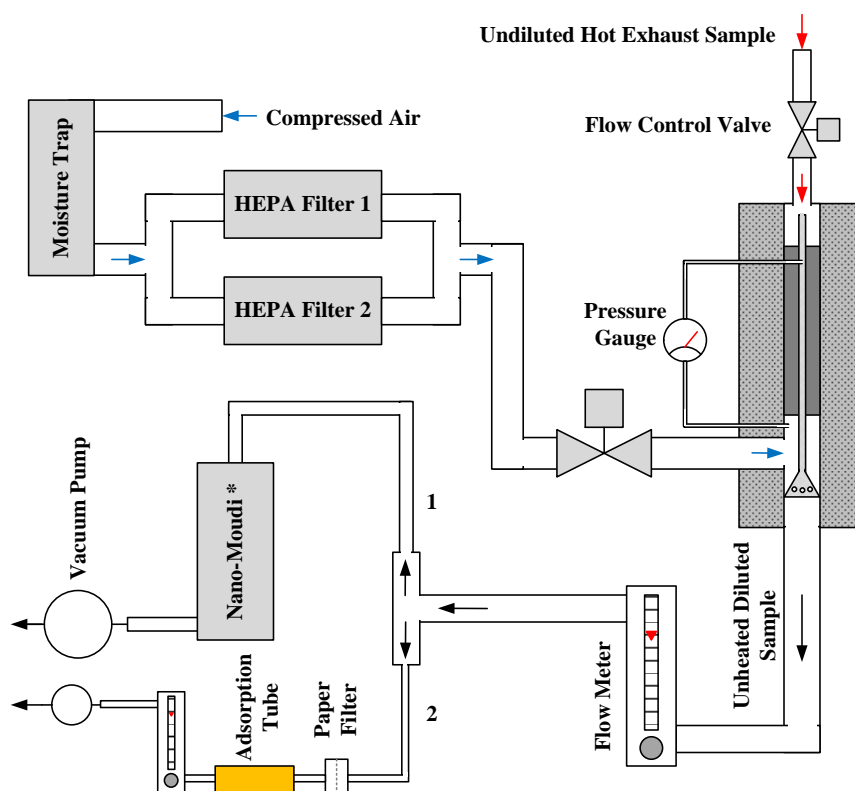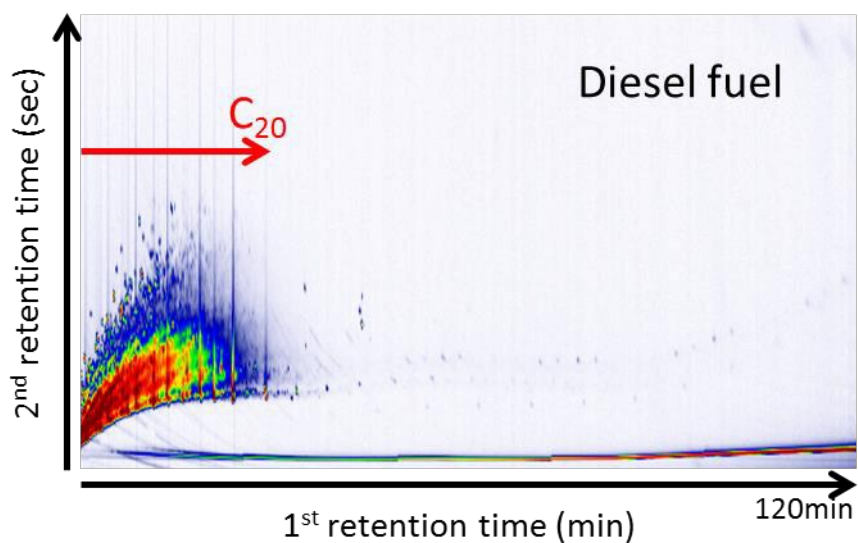
(A)
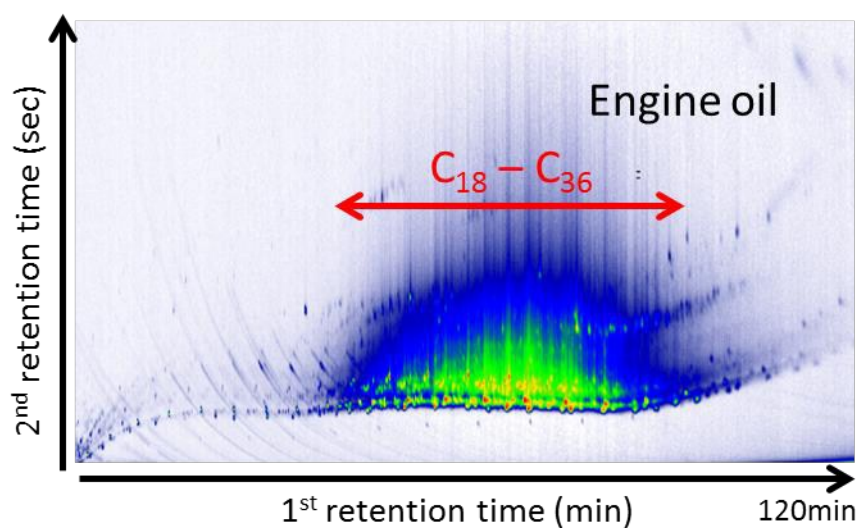
(B)

Figure 3. A two dimensional separation (contour plot) of **(A)** diesel fuel, and **(B)** engine lubricant. X-axis separation on a volatility basis; y-axis separation on a polarity basis. Each coloured spot represents an individual species and has a corresponding full mass spectrum. The intense red spots are major peaks, while the blue spots represent less abundant peaks.
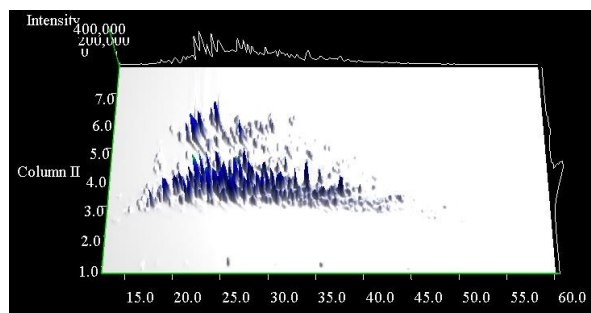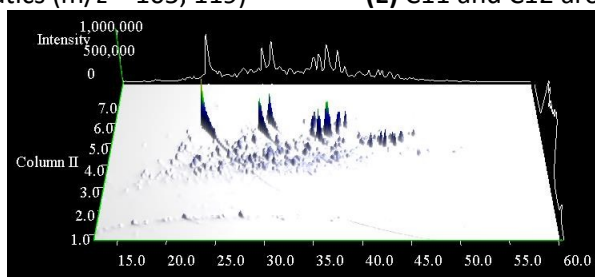
456

457

458

459

460
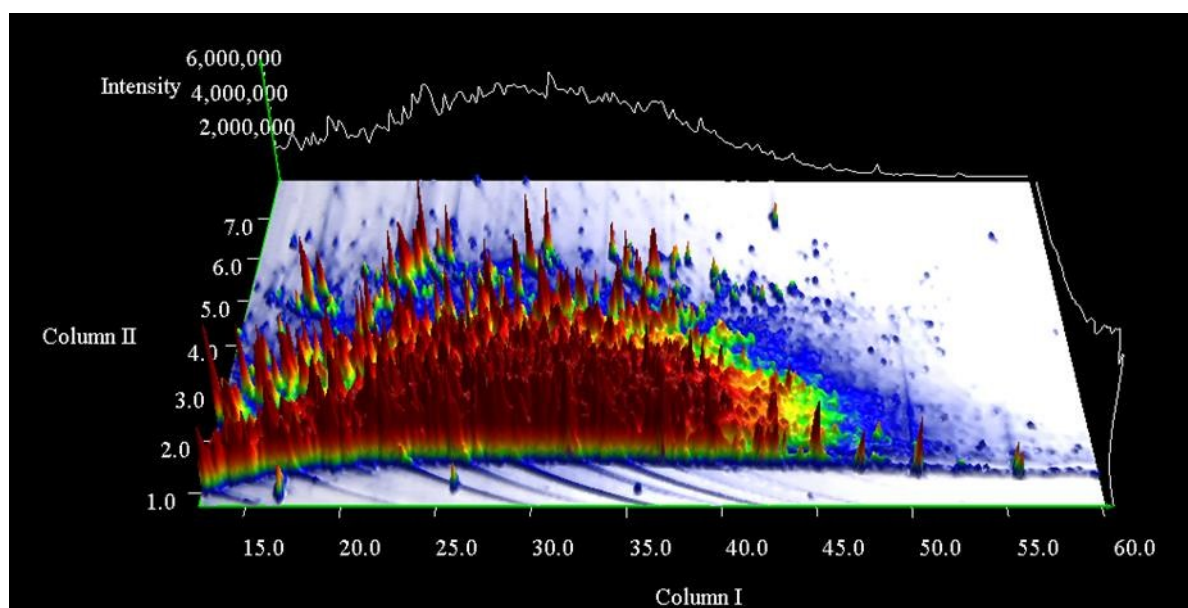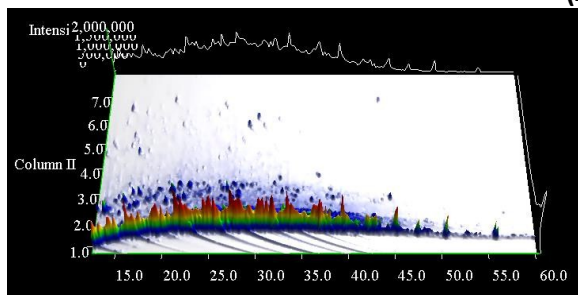
(A) TIC

(B) Straight & branched alkanes (m/z = 41, 57, 71)
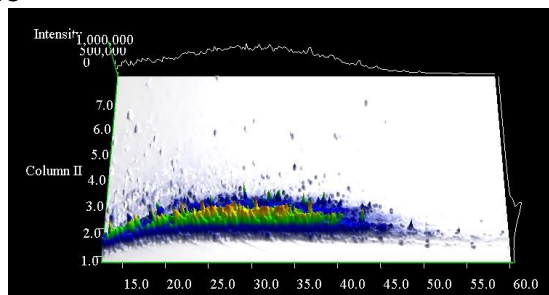
(C) cycloalkanes (m/z = 69, 82, 83, 97, 111)
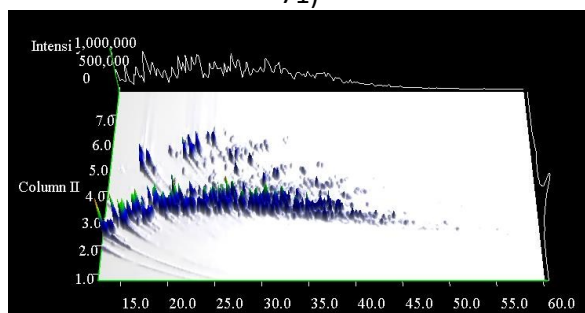
(D) C9 and C10 aromatics (m/z = 105, 119)

(E) C11 and C12 aromatics (m/z 133, 147)

(F) Naphthalenes (m/z = 128, 142, 156, 170, 184)

Figure 4. 3 dimensional separations of gas phase constituents collected with an adsorption tube and analysed using TD-GC×GC-ToF-MS. **(A)** Total ion chromatogram **(B)-(F)** Selected ion chromatograms. The white solid line signifies 1D chromatography.
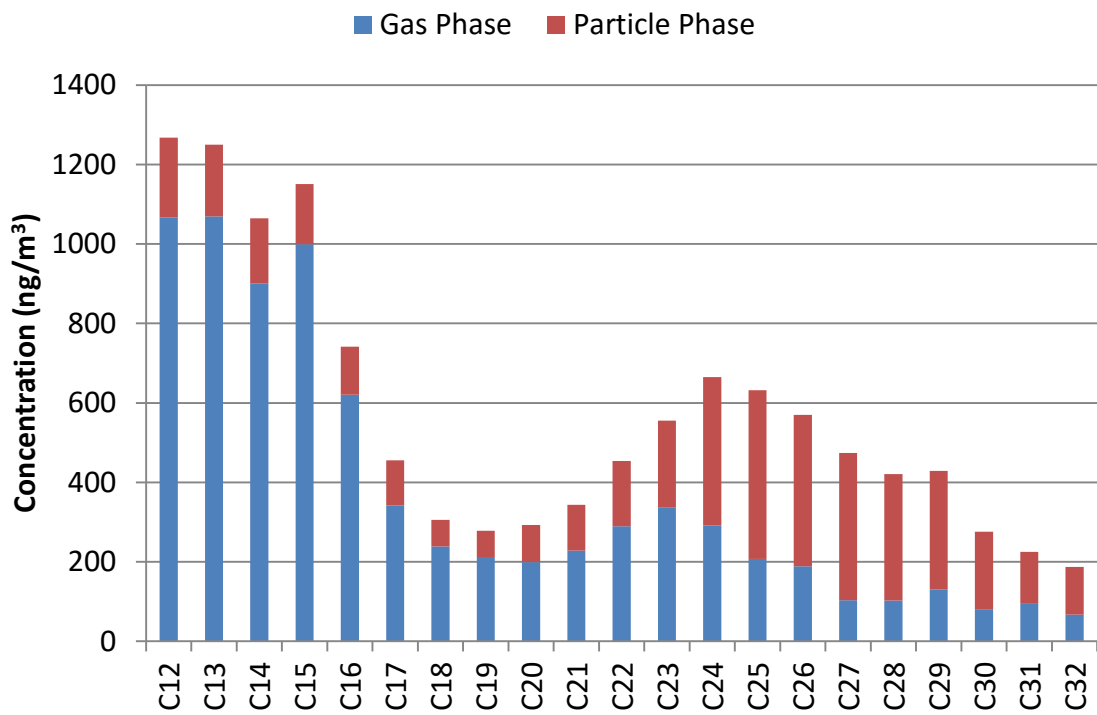
461

Figure 5. Gas/particle phase distribution of *n*-alkane concentration

462